Requirement of Heavy Neurofilament Subunit in the Development of Axons with Large Calibers

Gregory A. Elder,* Victor L. Friedrich, Jr.,‡ Chulho Kang,‡ Paolo Bosco,‡ Andrei Gourov,* Pang-Hsien Tu,§ Bin Zhang,§ Virginia M.-Y. Lee,§ and Robert A. Lazzarini‡

*Department of Psychiatry, ‡Brookdale Center for Developmental and Molecular Biology, Mount Sinai School of Medicine, New York, New York 10029; and §Center for Neurodegenerative Disease Research, Department of Pathology and Laboratory Medicine, University of Pennsylvania School of Medicine, Philadelphia, Pennsylvania 19104

Abstract. Neurofilaments (NFs) are prominent components of large myelinated axons. Previous studies have suggested that NF number as well as the phosphorylation state of the COOH-terminal tail of the heavy neurofilament (NF-H) subunit are major determinants of axonal caliber. We created NF-H knockout mice to assess the contribution of NF-H to the development of axon size as well as its effect on the amounts of low and mid-sized NF subunits (NF-L and NF-M respectively). Surprisingly, we found that NF-L levels were reduced only slightly whereas NF-M and tubulin proteins were unchanged in NF-H–null mice. However, the calibers of both large and small diameter myelinated axons were diminished in NF-H–null mice despite the fact that these mice showed only a slight decrease in NF density and that filaments in the mutant were most frequently spaced at the same interfilament distance found in control. Significantly, large diameter axons failed to develop in both the central and peripheral nervous systems. These results demonstrate directly that unlike losing the NF-L or NF-M subunits, loss of NF-H has only a slight effect on NF number in axons. Yet NF-H plays a major role in the development of large diameter axons.

Key words: neurofilament proteins • neuronal cytoskeleton • mice • knockout • gene targeting • large diameter axons

THE neuronal cytoskeleton consists of actin microfilaments, microtubules, and a network of 10-nm filaments, intermediate in size between the microfilaments and microtubules, termed intermediate filaments (IFs).[1] In the nervous system, at least seven different proteins contribute to the IF system (Liem, 1993; Xu et al., 1994). Three of these proteins, termed the neurofilament (NF) triplet, assemble into heteropolymeric NFs, which are the most prominent cytoskeletal components in large myelinated axons. Indeed, the NF triplet are the most abundantly expressed IF proteins in neurons. In mammals the triplet proteins, i.e., the light (NF-L), mid-sized (NF-M), and heavy (NF-H) NF subunits, have apparent molecular weights in SDS-PAGE gels of ~68,000, 150,000, and 200,000 kD, respectively. Each subunit protein is encoded by a separate gene (Julien et al., 1986; Lieberberg et al., 1989; Shniedman et al., 1988). Based on sequence homology and intron placement, the NF genes have been classified as type IV IFs along with α-internexin, which is also expressed in the nervous system (Chiu et al., 1989; Kaplan et al., 1990). Two type III IFs, peripherin (Greene, 1989) (expressed principally in some neurons of the peripheral nervous system) and vimentin (Cochard and Paulin, 1984) (expressed transiently in neuroepithelial stem cells) along with nestin (Lendahl et al., 1990) (a type VI IF expressed in neuroepithelial stem cells during early development) constitute the remaining IFs known to exist in neurons and neural progenitors in the mammalian nervous system.

The correlation between NF number in cross sections of mature axons and axonal caliber has long suggested a role for NFs as a major determinant of axonal diameter (Friede and Samorajski, 1970; Hoffman et al., 1985*a*,*b*, 1988). This correlation persists during axonal degeneration and regeneration (Hoffman et al., 1984) and changes in NF transport correlate temporally with alterations in the caliber of axons in regenerating nerves (Hoffman et al., 1985*b*). Additionally, fewer NFs are found at nodes of Ranvier where axonal diameter is reduced (Berthold, 1978).

Address all correspondence to R.A. Lazzarini, Brookdale Center for Developmental and Molecular Biology, Box 1126, Mount Sinai School of Medicine, New York, NY 10029. Tel.: (212) 241-4272. Fax: (212) 860-9279. E-mail: rlazzar@smtplink.mssm.edu

1. *Abbreviations used in this paper*: CNS, central nervous system; ES, embryonic stem; IF, intermediate filament; neo, neomycin; NF, neurofilament; NF-H, heavy neurofilament; NF-L, light neurofilament; NF-M, mid-sized neurofilament; PGK-1, phosphoglycerol kinase-1; PNS, peripheral nervous system.

Structurally, all IFs contain a relatively well-conserved α helical rod domain of ~310 amino acids with variable NH_2- and COOH-terminal regions (Steinert and Roop, 1986). In vitro, a network of 10-nm diameter filaments can be formed with NF-L alone or with combinations of NF-L/NF-M or NF-L/NF-H (Geisler and Weber, 1981; Liem and Hutchison, 1982). Additionally, NF-M and NF-H may form short homopolymeric filaments under some conditions (Balin et al., 1991*a*,*b*; Gardner et al., 1984). However, in vivo, rodent NFs appear to be obligate heteropolymers since none of the rat or mouse NF subunits can form filaments when transfected individually into cells lacking an endogenous IF network (Ching and Liem, 1993; Lee et al., 1993). Similar conclusions have also been reached by expressing rat NFs in an insect cell line that lacks endogenous IFs (Nakagawa et al., 1995) and in transgenic mice by forcing expression of mouse NFs in oligodendrocytes which normally lack IFs (Lee et al., 1993). These results argue that in vivo, rodent NFs are obligate heteropolymers requiring NF-L plus either NF-M or NF-H to form a filamentous network. However, NF assembly in other species may not always follow these rules since our own recent studies have shown that the human NF-L subunit can form homopolymers when expressed in a mammalian cell line that does not express any detectable IFs (Carter et al., 1998).

The precise mechanism by which NFs help determine axonal diameter remains incompletely understood. One striking feature of the NF-M and NF-H proteins is their long COOH-terminal tail regions. In this region the NF-H subunits (Lees et al., 1988; Lieberberg et al., 1989; Shneidman et al., 1988; Way et al., 1992) of all species examined have a series of lysine-serine-proline (KSP) repeats (43–52 in rodents and humans) in near perfect tandem arrays. The NF-M subunit (Levy et al., 1987; Myers et al., 1987; Napolitano et al., 1987; Zopf et al., 1987) may contain variable numbers of these repeated sequences depending on the species examined. For example, rodents (Levy et al., 1987; Napolitano et al., 1987) contain four dispersed repeats whereas human NF-M (Myers et al., 1987) contains a stretch of 12 nearly perfect repeats in a tandem array.

The KSP repeats of NF-H (and also when present in NF-M) have been shown to be major phosphorylation sites that account for the unusually high content of phosphoserine residues in these proteins (Lee et al., 1988). Both NFs in situ as well as filaments assembled in vitro appear to contain a core of all three subunits with sidearm projections composed of NF-M and NF-H (Hirokawa et al., 1984; Hisanaga et al., 1988; Mulligan et al., 1991). Phosphorylation of these sidearm projections in NF-M and NF-H is thought to modulate interfilament spacing and thereby contribute to the regulation of axonal caliber (Carden et al., 1987; de Waegh et al., 1992; Lee et al., 1988). Similar sidearms are not found in IFs composed of non-NF proteins such as keratins, vimentin, or glial fibrillary acidic protein (Heuser and Kirschner, 1980; Hirokawa and Heuser, 1981; Schnapp and Reese, 1982). Interestingly, the appearance of NF-H is delayed compared with the other NF subunits and it increases to appreciable levels only after birth (Carden et al., 1987; Shaw and Weber, 1982; Willard and Simon, 1983). Furthermore, the upregulation of NF-H coincides with the slowing of axonal transport and radial growth of the axons (Hoffman et al., 1985*a*,*b*).

To better define the role of the individual NF proteins in the growth and maintenance of axonal caliber, gene targeting techniques have been used to disrupt the NF genes in mice. Zhu et al. (1997) developed mice with a targeted disruption of the NF-L gene. These mice lacked axonal NFs, had diminished axonal calibers, and showed a delayed maturation of regenerating myelinated axons. Recently, we generated NF-M knockout mice (Elder et al., 1998). These mice lacked any overt behavioral phenotype or gross structural defects in the nervous system although the calibers of myelinated axons were markedly diminished. This reduction was likely the consequence of a drastic reduction in NF-L levels since axons of mutant animals contained less than half the normal number of NFs and an increased ratio of microtubules/NFs. These studies demonstrated that NF-M subunits mainly regulate axonal caliber by altering the level of NF-L and in turn the number of NFs in axons.

In the present study, we have generated NF-H knockout mice and we describe the effects of this null mutation on the expression of NF-L, NF-M, and microtubules, as well as the role of the NF-H subunit in specifying axonal diameter and its effect on interfilament spacing.

Materials and Methods

Generation of Targeting Vectors

Isologous genomic DNA for mouse NF-H was isolated from a 129 Sv/Ev genomic library prepared in λ Dash (Stratagene Inc., La Jolla, CA). Screening was with a probe from a previously isolated mouse genomic clone λ5a (Shneidman et al., 1988). A random primed PstI/NotI 430-bp probe (sequence −385 to +46) was used for initial screening and positive clones were rescreened with a 54-base oligonucleotide complementary to the immediate 5′ coding region of mouse NF-H. Restriction mapping confirmed that this clone was similar to the known structures of the mouse NF-H gene.

Targeting vectors were designed to use the positive and negative selection procedure described by Mansour et al. (1988). A map of the relevant portions of the NF-H gene and the targeting strategy is shown in Fig. 1 *A*. The neomycin resistance gene linked to the phosphoglycerol kinase-1 (PGK-1) promoter (540-bp) and PGK 3′ nontranslated sequence was derived from the plasmid pGEM7 (KJ1) Sal and the Herpes virus thymidine kinase gene also driven by the PGK-1 promoter was derived from the plasmid pGEM 7 (TK) Sal (both provided by R. Jaenisch, Whitehead Institute, Cambridge, MA).

Transfection and Screening of Embryonic Stem Cells and Generation of Chimeric Mice

Electroporations were performed in the R1 cell line (Nagy et al., 1993) and chimeric founders were generated as previously described (Elder et al., 1998). After electroporation, cells were plated in a nonselective media for 2 d and then selected in 150 μg/ml G418 (GIBCO BRL, Gaithersburg, MD) plus 2 μM ganciclovir (Syntex Research, Palo Alto, CA). After 10–14 d, neo-resistant colonies were established on feeder layers of mitomycin C–treated mouse embryonic fibroblasts in 96-well microtiter plates. Duplicate 96-well plates were established. One plate was frozen as described in Wurst and Joyner (1993) and the second was expanded into 24-well plates without feeder layers and DNA was prepared. Potentially targeted clones were screened by Southern blotting as described in Fig. 1.

Chimeras were generated by injecting embryonic stem (ES) cells into C57Bl/6 blastocysts at day 3.5 postcoitum and blastocysts were reimplanted into the uteri of pseudopregnant Swiss-Webster recipients at day 2.5 postcoitum. Chimeras were identified on the basis of agouti coat pigmentation. A male chimera was bred with a 129 Sv/J female. Heterozy-

gous offspring from this mating were subsequently bred with 129 Sv/J or Swiss-Webster females.

RNA Analysis

RNase protection assays were performed using uniformly labeled RNA probes synthesized with T3 or T7 RNA polymerase and 100 μCi of α-[^{32}P] UTP. Construction and use of mouse β-actin, NF-L, and NF-M probes in RNase protection assays have been previously described (Lee et al., 1992; Tu et al., 1995; Elder et al., 1998). An NF-H probe was constructed by cloning a PCR-amplified fragment of murine NF-H exon 3 into pBluescript II SK+ (Stratagene). This probe protects a 115-bp fragment from mouse NF-H (sequence 1,089–1,203 in Schneidman et al., 1988). The NF-H probe was hybridized to 10 μg of total brain RNA. After overnight hybridization at 45°C, samples were digested with RNase T1 (700 U/ml, Boehringer Mannheim Biochemicals, Indianapolis, IN) for 1 h at 30°C and then digested with proteinase K (125 μg/ml), phenol/chloroform extracted and ethanol precipitated. Protected fragments were separated on a 6% sequencing gel. After gel electrophoresis protected fragments were localized by autoradiography. Quantitative RNase protection assays for mouse NF-L and NF-M were performed as described in Tu et al. (1995) with NF-L and NF-M levels normalized to the expression of β-actin.

Quantitative Western Blot Analysis

Quantitative Western blots were performed as previously described (Tu et al., 1995) with minor modifications (Elder et al., 1998). Tissue was homogenized and sonicated in BUST buffer (50 mM Tris-HCl, pH 7.4, 8 M urea, 2% β-mercaptoethanol, and 0.5% SDS) and centrifuged at 40×10^3 rpm at 25°C for 30 min in a TL-100 ultracentrifuge (Beckman Instruments Inc., Fullerton, CA). Samples were loaded based on total protein levels or on a specific length of nerve segment. To generate blots based on total protein levels, 40 μg of total protein from neocortex or 10 μg of total protein from spinal cord were loaded in triplicates. To generate blots based on a specific length of nerve segment, sciatic nerve, L5 ventral roots, and optic nerves were removed and consecutive 2-mm-long segments from proximal to distal were cut. The second 2-mm-long nerve segments from NF-H–null and wild-type mice were individually homogenized in 35 μl (for optic nerve and ventral root) or 70 μl (for sciatic nerve) of BUST buffer. Blots were cut into three parts that were processed by incubating the top third overnight with RMO24 for detection of NFHP+++ or RMdO9 for NFHP−, the middle third with RMO189 for total NF-M or RMO55 for NFMP+++, and the lower third with a rabbit anti–NF-L polyclonal antiserum for total NF-L or a mouse anti–β-tubulin mAb (Amersham Pharmacia Biotech, Inc., Piscataway, NJ) for tubulin. Each part was then incubated for 1 h with 10 μCi ^{125}I-conjugated goat anti–mouse IgG for the mouse mAbs (RMO24, RMO55, RMO189, and anti–β-tubulin) or ^{125}I-conjugated Protein A for the rabbit anti–NF-L polyclonal antisera. The dried blots were exposed to PhosphorImager plates for various time periods and individual bands were visualized and quantified with ImageQuant software (all from Molecular Dynamics Inc., Sunnyvale, CA).

Electron Microscopy

Tissues were processed for electron microscopy by standard methods as previously described (Elder et al., 1998; Friedrich and Mugnaini, 1981). Mice were fixed by vascular perfusion with 2% formaldehyde (from paraformaldehyde), 1% glutaraldehyde, and 0.12 M sodium phosphate buffer, pH 7.4. Samples were postfixed in buffered osmium tetroxide, embedded in Epon, and then examined using a JEOL 100CX electron microscope (JEOL USA Inc., Peabody, MA).

NFs and microtubules were counted in cross sectional images of axons photographed at a magnification of 20,000 and enlarged an additional two and one-half-fold during printing. NF densities were determined as previously described (Elder et al., 1998) using methods similar to those described by Price et al. (1988). A template of hexagons (each equivalent to an actual area of 0.10 square microns) was placed on each print and the number of NFs that fell within each hexagon were counted. Nearest neighbor distances were computed from the x-y coordinates of NFs determined in representative electron micrographic prints.

Measurement of Axonal Diameters

Axonal diameters were measured as previously described (Elder et al., 1998) on 1-μm-thick transverse sections of L5 ventral root, sciatic nerve, or spinal cord. Sections were stained with toluidine blue and photographed with a Zeiss Axiophot microscope (Carl Zeiss Inc., Thornwood, NY). Photographic images were scanned into the program Adobe Photoshop 3.05 (Adobe Systems Inc., San Jose, CA) and enlarged three- to fourfold before printing. Optimal brightness and gray scale pixel values were adjusted so as to provide the sharpest discrimination of the myelin/axon border. Axon profiles were traced in nonoverlapping contiguous fields using a digitizing tablet and areas were determined using the program NIH Image (Bethesda, MD). Axons were assumed to be circular for purposes of diameter calculations. For sciatic nerves, all myelinated axons in the largest trunk of the nerve were numbered and every fifth myelinated axon was sampled chosen by a set of random numbers. Axons in spinal cord were measured in a 1.9×10^5 μm^2 area of the ventral medial portion of the third cervical segment as described in Elder et al. (1998). For optic nerve, random fields were photographed in the electron microscope at a magnification of 4,800 and enlarged an additional two and one-half-fold during printing. Every myelinated axon was sampled in four randomly chosen fields. Statistical analysis (unpaired *t* test or Mann–Whitney U test) was performed using the program StatView (Abacus Concepts Inc., Berkeley, CA).

Results

Production of Mice Bearing a Null Mutation in the NF-H Subunit

The targeting strategy for generating and screening NF-H mutant mice is illustrated in Fig. 1. A male chimera was bred with several C57BL/6 females to establish germ line transmission of the mutant NF-H allele. Male heterozygotes from these matings were subsequently bred with Swiss-Webster females. The male chimera was also bred with 129 Sv/J females to establish the mutation on the inbred 129 background. On all genetic backgrounds the mutant allele was transmitted in a Mendelian fashion. We have studied animals both on the inbred 129 background and on the mixed genetic background described above and have not detected any qualitative effects of genetic background on the phenotype of NF-H–null mutation.

RNase protection assays (Fig. 1 *D*) with an exon 3 probe revealed at most a faint NF-H RNA band in the NF-H–null mutant on long exposures of the autoradiogram. This most likely reflects a low-level hybrid neo/NF-H mRNA being produced off the PGK promoter. However, as shown in Fig. 1 *E* and Figs. 2 and 4, this mRNA does not produce any detectable full-length or truncated NF-H protein on Western blotting using a rabbit anti–NF-H polyclonal antiserum that is phosphorylation independent and is specific for an epitope at the extreme COOH terminus of NF-H as well as RMO24, a mouse monoclonal antibody against a highly phosphorylation-dependent epitope within the multiphosphorylation repeat domain of NF-H. We were also unable to detect NF-H protein immunocytochemically in brain sections from NF-H null mutant animals double labeled with a mouse monoclonal anti–NF-H antibody and a rabbit polyclonal anti NF-L antisera even though NF-L staining was present (data not shown).

NF-L and NF-M Levels in the NF-H–null Mutant

To determine if the absence of NF-H affected the levels of NF-L or NF-M, we performed quantitative Western blotting on NF-H–null, heterozygous, and control mice. Representative Western blots are shown in Fig. 2. The levels of NF-H were decreased in the neocorticies of heterozygous mice and were undetectable in those of NF-H–null mice.

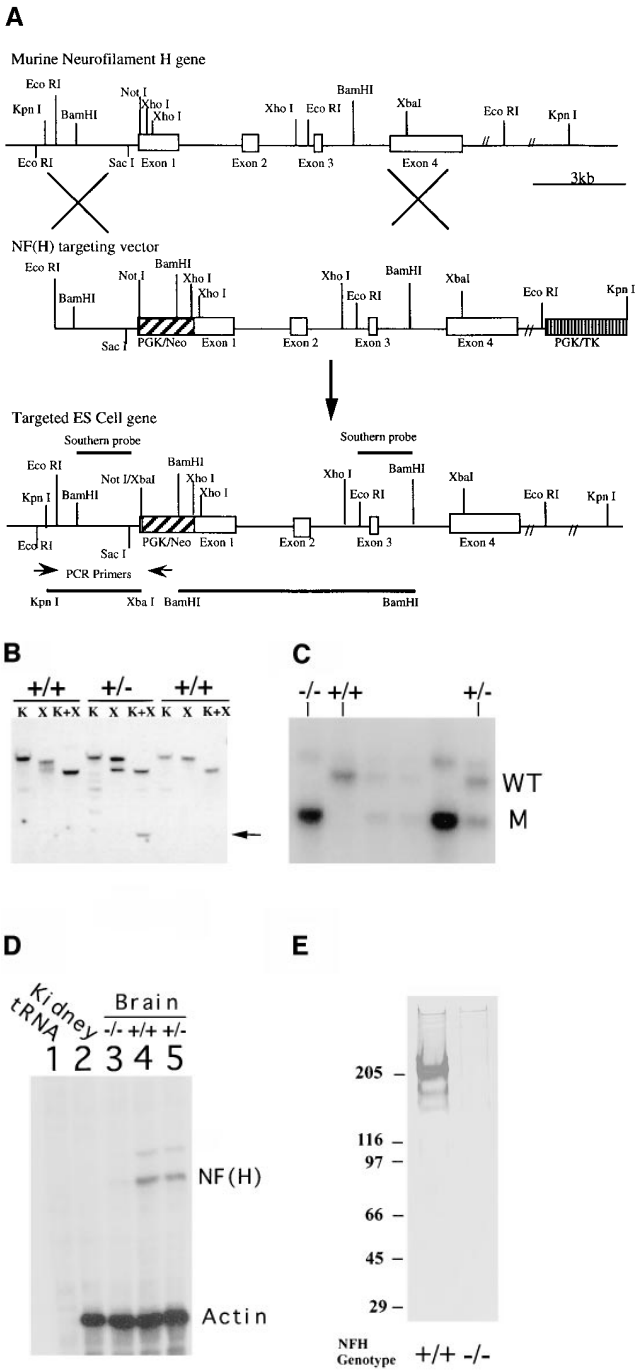

Figure 1. Targeted disruption of the mouse NF-H gene. (*A*) Targeting strategy for disruption of the mouse NF-H gene. The structure of the endogenous mouse NF-H (*A*) is shown in the top line. *Open boxes*, exons. A targeting vector designed to use positive and negative selection (Mansour et al., 1988) is shown in the center line. The PGK/neo gene was inserted in a sense orientation between NotI and XhoI sites (nucleotides −15 and +207 in Schneidman et al., 1988) in the first exon of mouse NF-H. The NF-H vector removes the initial ATG and the first 71 amino acids of the protein. It contains 2.1 kb of 5′ and 13.4 kb of 3′ homologous sequence and was linearized with KpnI. The overall targeting frequency was ~1 in 200 clones. (*B* and *C*) Southern blots of DNA from ES cells and mice with disrupted NF-H alleles. NF-H ES cell clones were screened by PCR using primers (*arrows* in *A*) derived from flanking 5′ NF-H sequence (5′-ATGGGCAAGGAAAGAGTCAGGG-3′) and from the PGK promoter (5′-TGGATGTGGAATGTGTGCGAGG-3′). The 2.4-kb PCR product was detected by Southern blotting. Suspected targeted clones based on PCR screening were digested with KpnI, XbaI, or KpnI/XbaI and probed with the BamHI/SacI 1,300-bp fragment shown in *A*. Successful targeting generates a 2.9-kb fragment caused by the introduction of an XbaI site at the 5′ end of the PGK/neo resistance gene. In *B*, a Southern blot is shown of a targeted ES cell clone digested with KpnI (*K*), XbaI (*X*), or KpnI/XbaI (*K*+*X*) double digest and probed with the BamHI/SacI fragment indicated above. Two clones show the expected wild-type pattern (+/+) whereas the targeted clone (+/−) gives an additional Xba band and a 2.9-kb Kpn/Xba band (*arrow*) consistent with homologous recombination. In *C*, a Southern blot of offspring from a heterozygous/heterozygous mating is shown. DNA was digested with BamHI and probed with the BamHI/EcoRI fragment indicated in *A*. Wild-type (*WT*) and mutant (*M*) bands are indicated. Examples of wild-type (+/+), heterozygous (+/−) and null mutant animals (−/−) are indicated. (*D*) RNA analysis of mutant animals. RNase protection assays were performed with 50,000 counts per minute (CPM) of a murine β-actin probe and 250,000 CPM of an exon 3 murine NF-H probe. Positions of the 115-bp NF-H and 65-bp actin-protected fragments are indicated. Lanes were hybridized with 15 μg of tRNA (lane *1*), 15 μg of total kidney RNA from a wild-type mouse (lane *2*), or 15 μg total brain RNA from a homozygous null mutant (−/−, lane *3*) and wild-type (+/+, lane *4*) or heterozygous littermates (+/−, lane *5*). (*E*) No detection of NF-H protein in NF-H–null mice. Western blotting was performed with RMO24 for detection of NFHP+++. No full-length or truncated NF-H protein could be detected in the spinal cord of NF-H −/− mice.

Quantitation of the Western blot data (Table I) showed that the immunoreactivities of both NFHP+++ and NFHP− decreased in the heterozygous mice by ~50%. These data suggest that the decreases in the NF-H immunoreactivities result from a decrease in the NF-H protein level rather than a change in the phosphorylation state. A similar decrease was also observed in spinal cord (Fig. 2 and Table I), hippocampus, brain stem, cerebellum, and sciatic nerve (data not shown).

Interestingly, unlike an NF-M–null mutant which had dramatic effects on NF-L levels (Elder et al., 1998), complete absence of the NF-H subunit produces at most a modest decrease in NF-L (~10–25%) and has essentially no effect on the levels of NF-M protein. Thus, these data strengthen the evidence that NF-M is the more important and central regulator of NF-L levels (Tu et al., 1995). As shown in Fig. 2 and Table I, the levels of β-tubulin were comparable to those of control mice, suggesting that the elimination of NF-H does not affect the amount of tubulin protein. Finally, using quantitative RNase protection assays, we observed no significant differences in the levels of NF-L or NF-M RNA in the brains of NF-H–null when compared with control mice (Fig. 3).

Diminished Axonal Diameters in NF-H Mutant Mice

The correlation between the number of NFs in cross sections of axons and axonal caliber has long suggested a role for NFs in establishing axonal diameter (Friede and Samorajski, 1970; Hoffman et al., 1988). This view has been reinforced by several recent animal models including NF-M and NF-L knockout mice which have shown that ra-

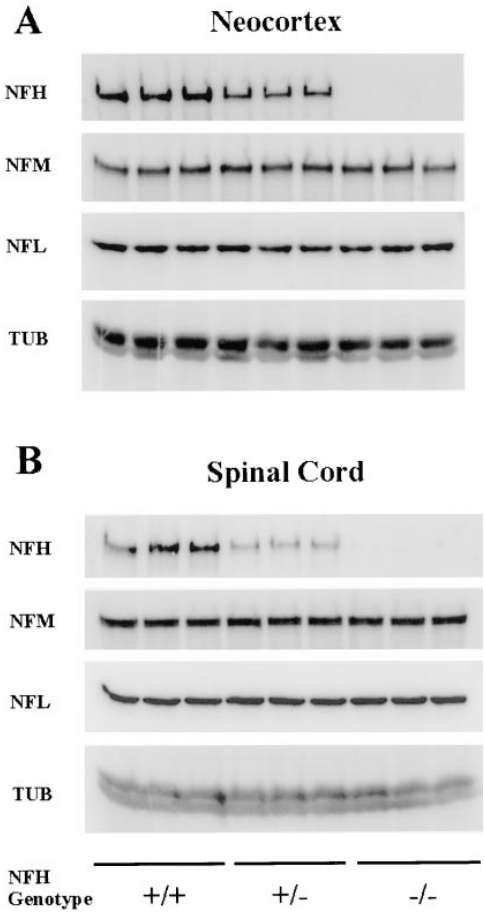

Figure 2. Quantitative Western blots of neocortex and spinal cord of NF-H heterozygous (+/−), NF-H null (−/−), and wild-type mice (+/+). Each sample was loaded in triplicate. The NF-H immunoreactivities are decreased in both neocortex and spinal cord of the heterozygous mice and are undetectable in the null mice. NFHP− is measured with RMdO9, a mAb against NF-H poorly or nonphosphorylated epitopes (Carden et al., 1987); NFHP+++ with RMO24, a mAb specific for highly phosphorylated epitopes, NF-M with RMO189 a mAb against the rod domain of NF-M; NF-L with a polyclonal rabbit anti-NF-L antiserum; TUB with a mAb specific for β–tubulin.

Table I. Summary of Quantitative Western Blot Analysis of NF-H Heterozygous and –null Mice

	Cortex		Spinal cord	
	Hetero/WT	Null/WT	Hetero/WT	Null/WT
NFHP−	0.54 ± 0.06	—	0.52 ± 0.08	—
NFHP+++	0.57 ± 0.11	—	0.67 ± 0.05	—
NFMPi	0.83 ± 0.07	0.93 ± 0.11	1.03 ± 0.11	0.96 ± 0.10
NFMP+++	0.75 ± 0.08	1.15 ± 0.19	1.10 ± 0.07	0.94 ± 0.08
NFL	0.75 ± 0.08	0.93 ± 0.12	0.93 ± 0.08	0.76 ± 0.03
Tubulin	0.96 ± 0.03	0.94 ± 0.06	1.10 ± 0.02	0.89 ± 0.01

Each value represents an average ± SEM of nine observations from three separate experiments. Data is presented as a ratio of heterozygous (*Hetero*) or null mutants relative to wild-type (*WT*) levels. NFHP− is measured with RMdO9, a mAb against poorly or nonphosphorylated NF-H epitopes; NFHP+++ with RM024, a mAb specific for highly phosphorylated epitopes of NF-H; NFMPi with RM0189, a mAb against the rod domain of NF-M; NFMP+++ with RMO55, a mAb specific for highly phosphorylated epitopes of NF-M; NF-L with a polyclonal rabbit anti–NF-L antiserum; tubulin with a mAb specific for β-tubulin.

dial growth of myelinated axons is inhibited in axons with a depleted NF content (Elder et al., 1998; Eyer and Peterson, 1994; Ohara et al., 1993; Yamasaki et al., 1991; Zhu et al., 1997).

To examine the effects of the NF-H–null mutation on axonal caliber, we measured the sizes of axons in two peripheral nervous system (PNS) nerves (i.e., L5 ventral root and sciatic nerve) and two central nervous system (CNS) structures (i.e., spinal cord and optic nerve). In addition, the NF protein in defined lengths of ventral roots, sciatic nerves, and optic nerves were also assessed. As shown in Fig. 4, *A* and *B*, the amount of NF-L protein detected in a defined length of all three nerves in the NF-H–null mice was only reduced by ~20% when compared with similar lengths of nerves from wild-type animals while the level of NF-M protein was essentially unchanged. By contrast, light microscopic examination of each region showed a generalized reduction in the size of myelinated axons with a concomitant increase in the number of smaller diameter fibers in the NF-H–null mutant. Examples of L5 ventral roots from 4-mo-old wild-type and null mutant animals are shown in Fig. 4 *C*. Although no significant change was found in the number of myelinated axons in NF-H–null mutant roots, myelinated axons appeared generally smaller in mutant roots with the largest diameter fibers in the mutant failing to reach the caliber of the largest axons in control. Average axonal diameter was decreased from 3.7 ± 1.4 (SD) μm in wild-type to 3.0 ± 1.0 μm in the NF-H mutant ($P < 0.0001$, Mann–Whitney U test). Examination of the frequency distribution of axonal diameters in control and mutant roots (Fig. 5 *A*) revealed that over 35% of myelinated axons in wild-type roots were larger than 4.0 μm, compared with only 14.9% in the null mutant. Only 2.6% of axons in the mutant reached diameters greater than 5.0 μm even though over 15% of this caliber axon were found in wild-type roots. The loss of large diameter myelinated axons was accompanied by a shift towards medium and

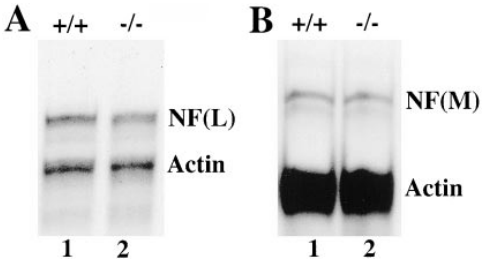

Figure 3. NF-L and NF-M RNA levels in NF-H–null mutant animals. (*A* and *B*) RNase protection assays to determine NF-L and NF-M RNA levels in the NF-H null mutant are shown. 5 μg of total brain RNA from a wild-type (lane *1*, +/+) or NF-H–null mutant (lane *2*, −/−) were hybridized with a murine β-actin probe and a mouse NF-L probe in *A* or a mouse NF-M probe in *B*. Protected fragments were separated as double-stranded RNA on 6% native polyacrylamide gels. Positions of the NF-L, NF-M, and β-actin bands are indicated. After normalization to the level of β-actin expression, neither NF-L nor NF-M RNA levels were significantly changed in the NF-H–null mutant.

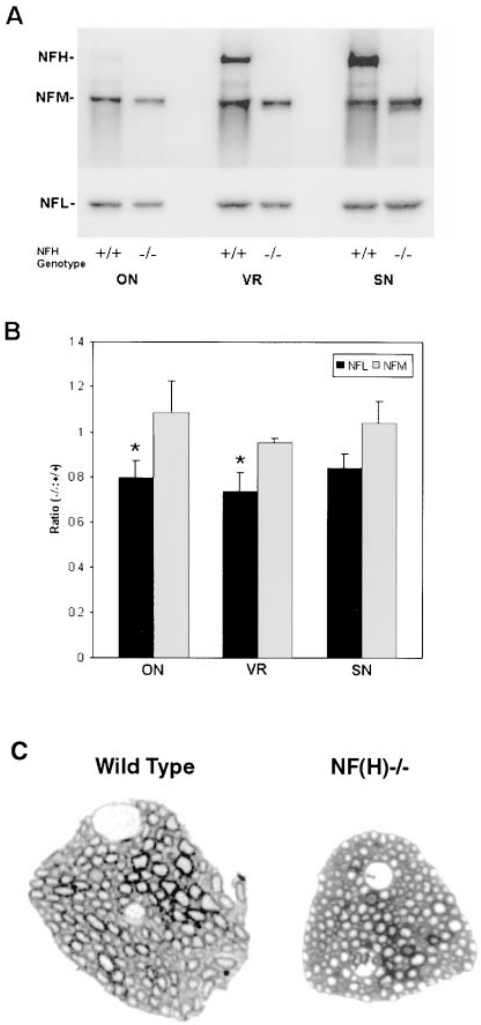

Figure 4. NF proteins in peripheral nerve and optic nerve and appearance of L5 ventral roots in NF-H–null mutant mice. (*A* and *B*) Western blots of sciatic nerves (*SN*), L5 ventral roots (*VR*), and optic nerves (*ON*) of 4-mo-old NF-H–null mutant (−/−) versus control mice (+/+). Quantification of immunoreactive protein bands was performed as described in Materials and Methods. 16 μl of extracts from the second 2-mm segment of each respective nerve were loaded into individual lanes of a 7.5% polyacrylamide gel and separated by SDS-PAGE. Proteins were then electrophoretically transferred to nitrocellulose membranes for quantitative Western blot analysis. NF-H immunoreactivity was visualized with RMO24 (phosphorylated NF-H–specific antibody); NF-M with RMO189 (phosphorylation-independent NF-M antibody), and NF-L with a rabbit anti–NF-L polyclonal antisera. Quantification of the Western blots (*B*) showed that the levels of NF-L protein significantly decreased in the ventral roots and optic nerves but not in sciatic nerves of NF-H −/− mice. The levels of NF-M proteins in the NF-H −/− mice remained comparable to those of +/+ mice. *, $P < 0.05$. (*C*) L5 ventral roots in wild-type and NF-H–null mutant mice. Light microscopy of toluidine blue–stained L5 ventral roots from 4-mo-old wild-type and NF-H–null mice. Note the reduced size of the NF-H mutant (−/−) root as well as the absence in the mutant of axons with calibers comparable to the largest present in the control.

small diameter fibers. We have also found axonal diameters to be reduced in NF-H heterozygous (+/−) mice to levels approximately intermediate between wild-type and null mutant animals (data not shown).

Similar changes were also seen in a morphometric analysis of axonal diameters in sciatic nerves from NF-H mutant and control animals (Fig. 5 *B*). Average diameters in a proximal segment of the nerve decreased from 3.6 ± 1.0 (SD) μm in wild type to 3.4 ± 1.1 μm in NF-H–null mutants ($P = 0.0145$, Mann–Whitney U test). The frequency distribution of axon diameters in sciatic nerves again revealed a shift towards small and medium-sized axons.

In the CNS, axonal diameters were also affected. In the ventral medial portion of the cervical cord (a region containing many large axons) the diameters of axons over 5 μm in size were decreased from 6.13 ± 1.91 μm in control to 5.28 ± 1.59 ($P < .0001$, Mann–Whitney U test, see Fig. 5 *C*). Likewise, in the optic nerves (an area of the CNS containing relatively small myelinated axons that are nearly all less than 2 μm in diameter), average axonal diameters decreased from 0.97 ± 0.30 μm in wild type to 0.91 ± 0.26 μm in NF-H–null mutants ($P = .0004$, Mann–Whitney U test). In both regions the frequency distribution of axonal diameters showed a shift towards smaller diameter fibers in the mutant mice (Fig. 5, *C* and *D*). Thus, the presence of the NF-H subunit is required to achieve maximal axonal caliber in all size classes of myelinated axons in both the CNS and PNS.

Neurofilament Content in Mice Lacking a Heavy NF Subunit

To look for an ultrastructural basis for the diminution of axonal diameters in the null mutant we examined NF and microtubule densities in electron micrographs of L5 ventral roots from mutant and control animals. NFs were readily apparent in both the null mutant and control (Fig. 6). Filaments in the mutant animal appeared to be of normal configuration and organization in both transverse and longitudinal sections (Fig. 6). Microtubules also appeared to be normal in appearance.

To determine if NF content was altered in the null mutants, NFs were counted in myelinated axons of a range of sizes and NF numbers were plotted against axonal area. As shown in Fig. 7 *A*, myelinated axons in the null mutant appeared to contain slightly fewer NFs than comparably sized axons in controls although microtubule numbers (Fig. 7 *B*) were unchanged.

To measure NF densities more directly in these same axons we used methods similar to those described by Price et al. (1988). NF densities were determined by applying a template of hexagons (every hexagon equivalent to an area of 0.10 square microns) over individual electron micrographs and counting the number of NFs in each hexagon. A frequency distribution plot was generated showing the number of NFs per hexagon (Fig. 7 *C*). The average number of NFs per hexagon was reduced from 15.7 ± 6.3 (SD) in control axons to 14.1 ± 6.3 in the mutant ($P = 0.0005$, unpaired t test) and as shown in Fig. 7 *C*, the frequency distribution was shifted in the mutant towards hexagons containing fewer NFs, demonstrating that NFs are slightly less densely packed in the NF-H.

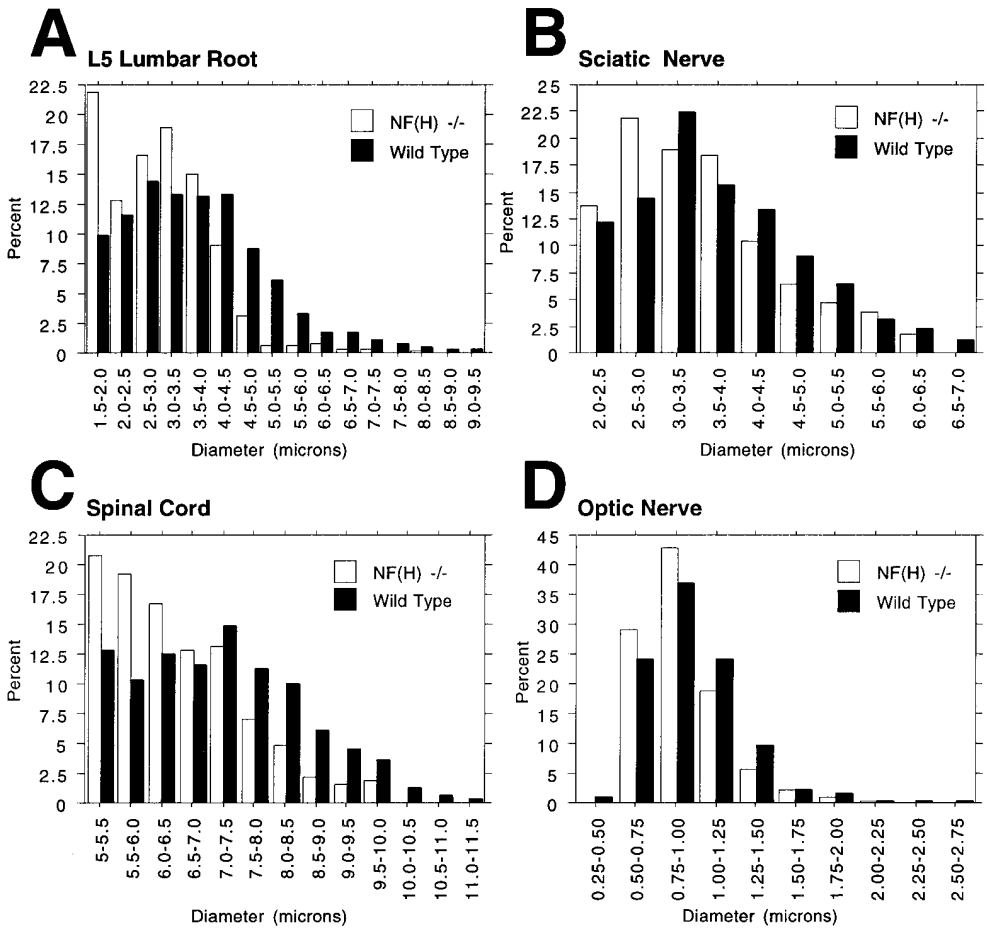

Figure 5. Axon calibers in NF-H–null mutant animals. (*A*) Diameters of all myelinated axons were measured in L5 ventral roots of 4-mo-old animals (n = 3 wild type, n = 3 mutant). Data is presented on all axons greater than 1.5 μm in diameter. Note the marked reduction of axons greater than 5 μm in diameter in the mutant accompanied by an increase in smaller diameter fibers. (*B*) Axon diameters were measured in the sciatic nerve of a 2-mo-old wild-type and mutant animal. Quantitation was performed by sampling every fifth myelinated axon in the largest trunk of a proximal portion of the nerve. Data is presented for all axons greater than 2 μm in diameter (n = 374, wild type, 313 NF-H −/−). Note the shift to smaller diameter fibers in the null mutant. (*C*) Axon sizes were measured in a 1.9×10^5 μm^2 area of the ventral medial portion of the third cervical segment. This region was chosen since comparable areas could be easily identified in different animals and because this region contains many large axons. Data is presented for all axons greater than 5 μm in diameter (n = 311 for wild type and 620 for NF-H −/−) from a 2-mo-old wild-type and NF-H −/− animal. Note the dramatic reduction in large diameter fibers accompanied by a shift to smaller diameter axons in the null mutant. (*D*) Axon sizes were determined in the optic nerves of 2-mo-old wild-type and NF-H–null mutant animals. Quantitation was performed on electron micrographs of optic nerve by measuring every myelinated axon in four randomly selected fields (n = 686 wild type, 741 NF-H −/−). Note the shift towards smaller diameter axons in the mutant.

To examine the effect of the lack of NF-H on interfilament spacing, we measured nearest neighbor distances in axons from wild-type and NF-H–null mice (Fig. 8). Mean nearest neighbor distances increased from 45 ± 18 (SD) nm in control to 50 ± 20 in the mutant ($P < 0.0001$, Mann–Whitney U test). Yet despite the increased mean interfilament distance, the modal nearest neighbor distance was identical in both mutant and wild type (47 nm). Thus, although average interfilament distances were increased (as would be expected if filament number was decreased), when filaments are closely spaced in the mutant they assume an interfilament distance that is similar to wild type.

Lack of Overt Phenotype or Major Structural Defects in Mice with a Disrupted NF-H Gene

No gross phenotype resulted from a null mutation in the NF-H gene. Animals appeared normal at birth and mutant animals up to 1 yr of age have shown no obvious health problems. Light microscopy has revealed no obvious morphogenetic defects in either CNS or PNS development.

Discussion

Several recent animal models have clearly demonstrated that axonal NFs are not essential for the survival of small animals (Eyer and Peterson, 1994; Ohara et al., 1993; Zhu et al., 1997). Yet the highly conserved nature of NF proteins suggests that they serve some important function. NFs have long been suspected to help specify the diameter of axons and to support their integrity (Hoffman et al., 1988) and these same animal models (Eyer and Peterson, 1994; Ohara et al., 1993; Zhu et al., 1997) have clearly shown that radial growth is impaired in axons lacking NFs. However, how NFs increase axon caliber and what role individual subunits play in this process remains to be clarified. Myelin-forming cells may also influence axonal diameter through affects on the amount and phosphorylation state of NF subunits (Cole et al., 1994; de Waegh et al., 1992; Hsieh et al., 1994; Nixon et al., 1994; Yin et al., 1998). Thus, NFs may function as effector proteins subject to a complex regulatory cross-talk between neurons and myelinating Schwann cells or oligodendrocytes.

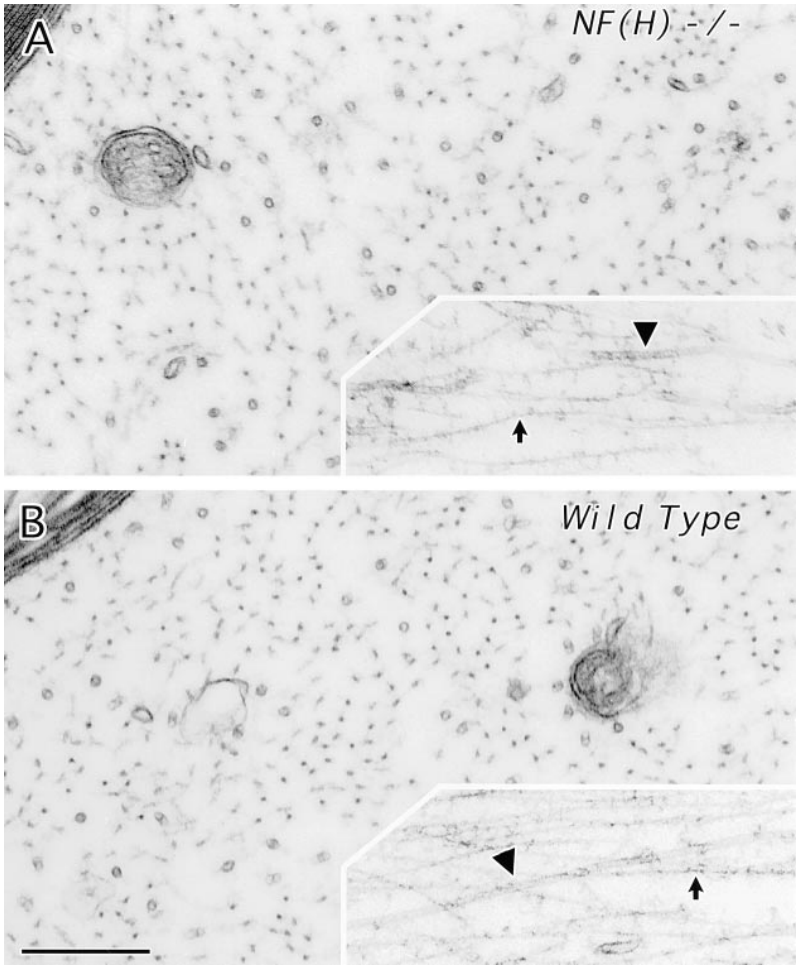

Figure 6. Fine structure of axons in mice with an NF-H–null mutation. (*A* and *B*) Axons of L5 ventral root are viewed in cross section and longitudinally (*insets*) from an NF-H–null mutant (*A*) or wild-type mouse (*B*). Axoplasm, including neurofilaments (*arrows*) and microtubules (*triangles*), appears normal in the NF-H–null mutant (*A*) as compared with control (*B*). Bar, 300 nm.

Evidence for the in vivo function of NF-L has come from studies of a Japanese quail (Quiver) with a nonsense mutation in the NF-L gene (Ohara et al., 1993) and from mice whose NF-L gene was disrupted by gene targeting (Zhu et al., 1997). In the homozygous state, the Quiver quail contains no axonal NFs and exhibits a mild generalized quivering (Yamasaki et al., 1993). Radial growth of myelinated axons is severely attenuated with a consequent reduction in axonal conduction velocity (Sakaguchi et al., 1993). Mice with a targeted disruption of the NF-L gene (Zhu et al., 1997) are also deficient in axonal NFs and have diminished axonal calibers. Interestingly, myelinated axons in NF-L knockout mice regenerated more slowly after axotomy emphasizing that NFs are required for the normal regeneration of axons. In transfected cells, both rodent (Ching and Liem, 1993; Lee et al., 1993) and human (Carter et al., 1998) NFs require the presence of NF-L if filaments containing NF-M and NF-H are to form in cells lacking an endogenous IF network. The depletion of axonal NFs in both NF-L mutant quail and NF-L–null mice supports the notion that NF-L is required for the formation of 10-nm-diam filaments in many species. Interestingly, overexpression of NF-L alone in transgenic mice leads to an increase in packing density of axonal NFs, but no increase in axonal caliber (Monteiro et al., 1990). This observation points to an important role for other NF subunits in determining axonal caliber as well. Thus, the most important function of NF-L may well be its ability to stimulate filament formation.

The most direct evidence for the role of NF-M comes from a previous NF-M–null mutation generated by gene targeting (Elder et al., 1998). In these mice the calibers of myelinated axons were diminished and additionally, NF-L levels were dramatically decreased and NF-H levels were increased slightly. Axons of mutant animals contained less than half the normal number of NFs and an increased ratio of microtubules to NFs. These studies demonstrate that NF-M is required if myelinated axons are to achieve maximal diameters and they also support previous studies demonstrating that NF-M regulates the level of NF-L (Tu et al., 1995). However, in mice overexpressing human NF-M protein (Tu et al., 1995), increased levels of NF-M alone also failed to increase axonal caliber possibly due to a concomitant decrease in the phosphorylation state of NF-H offsetting the effects of increasing NF-M levels. In studies by Xu et al. (1996), overexpression of mouse NF-M in transgenic mice actually decreased axonal diameter. These results seem best explained as a perturbation of NF stoichiometry in which overexpression of NF-M leads to the formation of perikaryal NF inclusions in motor neurons and the depletion of NFs from axons. Consistent with this explanation these same studies (Xu et al., 1996) found that

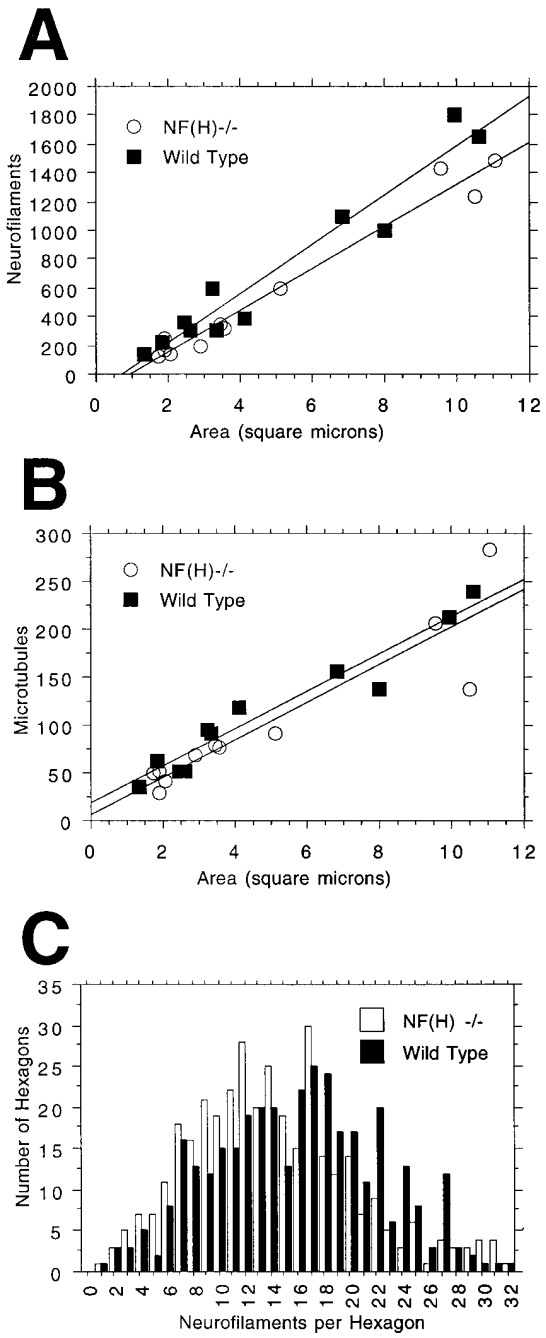

Figure 7. Neurofilament and microtubule content in NF-H–deficient animals. (*A*) NFs were counted in myelinated axons of L5 ventral root axons of 4-mo-old wild-type and control animals. The number of NFs in each axon was plotted against axonal size (area in square microns). Note that in myelinated axons of similar size the wild type has slightly more NFs than the NF-H–null mutant. (*B*) Microtubules were counted in the same axons as in *A*. No significant difference between mutant and control was found in the number of microtubules. (*C*) NF densities were determined using methods similar to those described by Price et al. (1988). A template of hexagons was applied over each electron micrograph and the number of NFs per hexagon counted in all hexagons, which fell completely within axonal borders. Hexagons were excluded only if vesicular organelles filled more than ~10% of the hexagon. At least 300 hexagons (n = 351 wild type, 357 NF-H mutant) each equivalent to an area of 0.10 square microns were counted and a frequency distribution plot was generated showing the number of NFs per hexagon. Note the reduced density of NFs in the NF-H mutant.

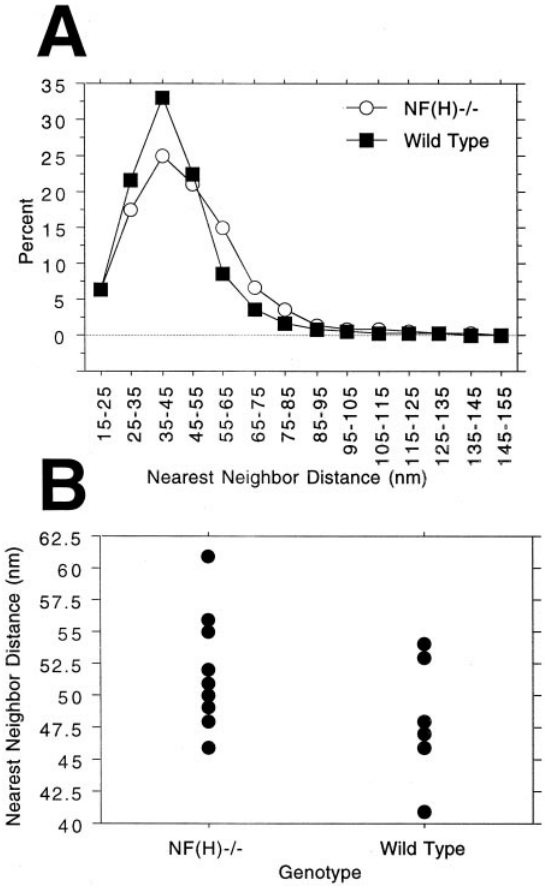

Figure 8. Nearest neighbor analysis of NF spacing in NF-H–deficient animals. (*A*) Interfilament spacing was analyzed in 10 mutant (range 1.88–11.08 square microns, average 5.29 ± 3.64 SD) and 10 wild-type (range 1.33–10.59, average 4.62 ± 3.33) axons from the L5 ventral root of 4-mo-old animals. The positions of all NFs in each axon cut in true cross section (n = 4,708 mutant and 4,965 wild type) were determined and nearest neighbor distances computed. Note that although the decreased NF density in the mutant results in an increased average interfilament distance, the modal distance is similar in both mutant and control. (*B*) Values for the individual axons measured in *A* are shown.

overexpression of NF-M (or NF-H) in combination with NF-L increased radial growth of axons, arguing that NF-M or NF-H must coassemble into filaments with NF-L before they can effect the radial growth of axons.

Our present studies show that the NF-H subunit is also needed if axons are to develop maximal calibers. In both the CNS and PNS, relatively large diameter axons were shifted into mid-sized axons while mid-sized axons became small axons. It is interesting to note that this effect is particularly prevalent in the large myelinated axons. The largest caliber axons disappeared in the lumbar ventral roots with a concomitant increase in smaller-sized axons. A similar effect is also seen in NF-M–null mutant mice (Elder et al., 1998). However, our data show that NF-M and NF-H regulate axonal caliber through fundamentally different mechanisms. In NF-M–null mice, reduced axonal caliber is associated with a greater than 50% reduction in NF number whereas NF-L and NF-H protein levels in nerve fall to

about half of control (Elder et al., 1998). Whereas in the NF-H–null mutation, there is only a slight reduction in NF number per axon (~10% fewer) while NF-L protein levels per unit length of nerve are ~20% less and NF-M levels are essentially unchanged. Yet a proportionately similar effect is seen on average axonal caliber (in both cases an ~20% reduction in the L5 ventral roots of 4-mo-old NF-M or NF-H–null mutant animals). Thus, the conspicuous absence of axons with the largest caliber cannot be accounted for by the small decrease in NF proteins in the NF-H null mutant nerves. Rather, these data suggest that NF-H plays some unique role in expanding axonal caliber that cannot be correlated directly with NF number.

The slight depletion of filaments likely accounts for the increased average nearest neighbor distances in NF-H–null mutant axons (45 nm in control versus 50 nm in mutant). However, it is interesting that filaments in the mutant most frequently occur 47 nm from their nearest neighbor (the modal distance) identical to that found in control. A similar effect was also seen in the NF-M–null mutant in which an even more extensive depletion of NFs had occurred (Elder et al., 1998). Such observations argue that associative interactions may be occurring between filaments since in either mutant when filaments are closely spaced (e.g., less than 60 nm) they assume a characteristic interfilament distance. The nature of these associative interactions is unknown but apparently does not require the presence of both NF-M and NF-H.

It is possible that the lack of NF-H affects other physiological processes such as axonal transport, and these may be important but are not addressed in this study. Initially, NF-L and NF-M are coexpressed whereas NF-H appears later (Carden et al., 1987; Shaw and Weber, 1982). This delayed expression of NF-H correlates developmentally with the slowing of axonal transport that normally occurs as axons mature (Willard and Simon, 1983). Such observations have led to the suggestion that an immature form of NFs composed of NF-L and NF-M might function in establishing the early neuronal phenotype and in maintaining neurite outgrowth. Addition of NF-H might confer a "mature" phenotype and be important in modulating axonal events such as the slowing of NF transport and the radial growth of axons. The mice described here will be a valuable tool to understand the role of NF-H in axonal transport and axonal maturity. Another function of NF-H could be in the stabilization of the axon and/or conduction velocity. In this regard, studies on the NF-H null mice as a function of aging and/or physical stress may provide some insight into the role of NF-H in neurodegeneration. Future studies in these animals promise to yield additional insights into the mechanisms that regulate NF assembly as well as leading to further clarification of the normal function of NFs and their role in neurodegenerative diseases.

We thank C. Li, Z. Liang, and H. O'Sullivan (Mt. Sinai School of Medicine, New York, NY) for technical assistance. We also thank R. Jaenisch (Whitehead Institute, Cambridge, MA) and K. Andrikopoulos (Mt. Sinai School of Medicine) for gifts of PGK/TK and PGK/neo plasmids, K. Andrikopoulos for the gift of a 129 Sv/Ev mouse genomic library, and A. Nagy (Mt. Sinai Hospital, Toronto, Canada) for the gift of R1 cells. R. Gordon (Mt. Sinai School of Medicine) is thanked for assistance with electron microscopy and J. Reinitz (Mt. Sinai School of Medicine) for assistance with nearest neighbor analysis. We would also like to thank B. Gibasson (University of Pennsylvania School of Medicine, Philadelphia, PA) for critically reading the manuscript.

This work was supported by grants from the American Health Assistance Foundation and the Amyotrophic Lateral Sclerosis Association G.A. Elder, National Institute of Neurological Disorders and Stroke to V.M.-Y. Lee (NS18616), and NIA to R.A. Lazzarini (P50 AG 05138-11).

Received for publication 5 May 1998 and in revised form 5 August 1998.

References

Balin, B.J., E.A. Clark, J.Q. Trojanowski, and V.M.-Y. Lee. 1991. Neurofilament reassembly in vitro: biochemical, morphological and immuno-electron microscopic studies employing antibodies to defined epitopes. *Brain Res.* 556:181–195.

Balin, B.J., and V.M.-Y. Lee. 1991. Individual neurofilament subunits reassembled in vitro exhibit unique biochemical, morphological and immunological properties. *Brain Res.* 556:196–208.

Berthold, C.-H. 1978. Morphology of normal peripheral axons. *In* Physiology and Pathobiology of Axons. S.G. Waxman, editor. Raven Press, New York. 3–63.

Carden, M.J., J.Q. Trojanowski, W.W. Schleapfer, and V.M.-Y. Lee. 1987. Two-stage expression of neurofilament polypeptides during rat neurogenesis with early establishment of adult phosphorylation. *J. Neurosci.* 7:3489–3504.

Carter, J., A. Gragerov, K. Konvicka, G. Elder, H. Weinstein, and R.A. Lazzarini. 1998. Neurofilament (NF) assembly; divergent characteristics of human and rodent NF-L subunits. *J. Biol. Chem.* 273:5101–5108.

Ching, G., and R. Liem. 1993. Assembly of type IV neuronal intermediate filaments in nonneuronal cells in the absence of preexisting cytoplasmic intermediate filaments. *J. Cell Biol.* 122:1323–1335.

Chiu, F.-C., E.A. Barnes, K. Das, J. Haley, P. Socolow, F.P. Macaluso, and J. Fant. 1989. Characterization of a novel 66 kDa subunit of mammalian neurofilaments. *Neuron.* 2:1435–1445.

Cochard, P., and D. Paulin. 1984. Initial expression of neurofilaments and vimentin in the central and peripheral nervous system of the mouse embryo in vivo. *J. Neurosci.* 4:2080–2094.

Cole, J.S., A. Messing, J.Q. Trojanowski, and V.M.-Y. Lee. 1994. Modulation of axon diameter and neurofilaments by hypomyelinating Schwann cells in transgenic mice. *J. Neurosci.* 14:6956–6966.

de Waegh, S., V.M.-Y. Lee, and S.T. Brady. 1992. Local modulation of neurofilament phosphorylation, axonal caliber, and slow axonal transport by myelinating Schwann cells. *Cell.* 68:451–463.

Elder, G.A., V.L. Friedrich, P. Bosco, C. Kang, P.-H. Tu, V.M.-Y. Lee, and R.A. Lazzarini. 1998. Absence of the mid-sized neurofilament subunit decreases axonal diameter, levels of light neurofilament (NF-L) and neurofilament content. *J. Cell Biol.* 141:727–739.

Eyer, J., and A. Peterson. 1994. Neurofilament-deficient axons and perikaryal aggregates in viable transgenic mice expressing a neurofilament-β galactosidase fusion protein. *Neuron.* 12:389–405.

Friede, R., and T. Samorajski. 1970. Axon caliber related to neurofilaments and microtubules in sciatic nerve. *Anat. Rec.* 167:379–388.

Friedrich, V.L.J., and E. Mugnaini. 1981. Preparation of neural tissues for electron microscopy. *In* A Handbook of Neuroanatomical Tract Tracing Techniques. L. Heimer and M. Robards, editors. Plenum Press, New York. 377–406.

Gardner, E.E., D. Dahl, and A. Bignami. 1984. Formation of 10 nm filaments from the 150 K-dalton neurofilament protein. *J. Neurosci. Res.* 11:145–155.

Geisler, N., and K. Weber. 1981. Self-assembly in vitro of 68,000 molecular weight component of the mammalian neurofilament triplet proteins into intermediate size filaments. *J. Mol. Biol.* 151:565–571.

Greene, L.A. 1989. A new neuronal intermediate filament protein. *Trends Neurosci.* 12:228–230.

Heuser, J.E., and M. Kirschner. 1980. Filament organization revealed in platinum replicas of freeze-dried cytoskeletons. *J. Cell Biol.* 86:212–234.

Hirokawa, N., and J.E. Heuser. 1981. Quick-freeze, deep-etch visualization of the cytoskeleton beneath surface differentiations of intestinal epithelial cells. *J. Cell Biol.* 91:399–409.

Hirokawa, N., M.A. Glicksman, and M.B. Willard. 1984. Organization of mammalian neurofilament polypeptides within the neuronal cytoskeleton. *J. Cell Biol.* 98:1523–1536.

Hisanaga, S., and N. Hirokawa. 1988. Structure of the peripheral domains of neurofilaments revealed by low angle rotary shadowing. *J. Mol. Biol.* 202: 297–305.

Hoffman, P.N., J.W. Griffin, and D.L. Price. 1984. Control of axonal caliber by neurofilament transport. *J. Cell Biol.* 99:705–714.

Hoffman, P.N., E.H. Koo, N.A. Muma, J.W. Griffin, and D.L. Price. 1988. Role of neurofilaments in the control of axonal caliber in myelinated nerve fibers. *In* Intrinsic Determinants of Neuronal Form and Function. Vol. 37. R.J. Lasek and M.M. Black, editors. Alan R. Liss, New York. 389–402.

Hoffman, P.N., J.W. Griffin, B.G. Gold, and D.L. Price. 1985*a*. Slowing of neurofilament transport and the radial growth of developing nerve fibers. *J. Neurosci.* 5:2920–2929.

Hoffman, P.N., G.W. Thompson, J.W. Griffin, and D.L. Price. 1985*b*. Changes

in neurofilament transport coincide temporally with alterations in the caliber of axons in regenerating motor fibers. *J. Cell Biol.* 101:1332–1340.
Hsieh, S.-T., G.J. Kidd, T.O. Crawford, Z. Xu, W.-M. Lin, B.D. Trapp, D.W. Cleveland, and J.W. Griffin. 1994. Regional modulation of neurofilament organization by myelination in normal axons. *J. Neurosci.* 14:6392–6401.
Julien, J.-P., D. Meyer, D. Flavell, J. Hurst, and F. Grosveld. 1986. Cloning and developmental expression of the murine neurofilament gene family. *Mol. Brain Res.* 1:243–250.
Kaplan, M.P., S.S.M. Chin, K.H. Fliegner, and R.K.H. Liem. 1990. α-internexin, a novel neuronal intermediate filament protein, precedes the low molecular weight neurofilament (NF-L) in the developing rat brain. *J. Neurosci.* 10: 2735–2748.
Lee, M., Z. Xu, P. Wong, and D. Cleveland. 1993. Neurofilaments are obligate heteropolymers in vivo. *J. Cell Biol.* 122:1337–1350.
Lee, V.M.-Y., G.A. Elder, L.-C. Chen, Z. Liang, S.E. Snyder, V.L. Friedrich, and R.A. Lazzarini. 1992. Expression of human mid-sized neurofilament subunit in transgenic mice. *Mol. Brain Res.* 15:76–84.
Lee, V.M.-Y., L. Otvos, Jr., M. Carden, M. Hollosi, B. Dietzschold, and R.A. Lazzarini. 1988. Identification of the major multiphosphorylation site in mammalian neurofilaments. *Proc. Natl. Acad. Sci. USA*. 85:1998–2002.
Lees, J.F., P.S. Shneidman, S.F. Skuntz, M.J. Carden, and R.A. Lazzarini. 1988. The structure and organization of the human heavy neurofilament subunit (NF-H) and the gene encoding it. *EMBO (Eur. Mol. Biol. Organ.) J.* 7:1947–1955.
Lendahl, U., L.B. Zimmerman, and D.G. McKay. 1990. CNS stem cells express a new class of intermediate filament protein. *Cell.* 60:585–595.
Levy, E., R.K.H. Liem, P. D'Eustachio, and N.J. Cowan. 1987. Structure and evolutionary origin of the gene encoding mouse NF-M, the middle-molecular-mass neurofilament protein. *Eur. J. Biochem.* 166:71–77.
Lieberberg, I., N. Spinner, S. Snyder, J. Anderson, D. Goldgaber, M. Smulowitz, Z. Carroll, B. Emanuel, J. Breitner, and L. Rubin. 1989. Cloning of a cDNA encoding the rat high molecular weight neurofilament peptide (NF-H): developmental and tissue expression in the rat, and mapping of its human homologue to chromosome 1 and 22. *Proc. Natl. Acad. Sci. USA*. 86:2463–2467.
Liem, R., and S. Hutchison. 1982. Purification of individual components of the neurofilament triplet proteins into intermediate size filaments: filament assembly from the 70,000 dalton subunit. *Biochemistry*. 21:3221–3226.
Liem, R.K.H. 1993. Molecular biology of neuronal intermediate filaments. *Curr. Opin. Cell Biol.* 5:12–16.
Mansour, S.L., K.R. Thomas, and M.R. Capecchi. 1988. Disruption of the proto-oncogene int-2 in mouse-derived stem cells: a general strategy for targeting mutations to non-selectable genes. *Nature*. 336:348–352.
Monteiro, M.J., P.N. Hoffman, J.D. Gearhart, and D.W. Cleveland. 1990. Expression of NF-L in both neuronal and nonneuronal cells of transgenic mice: increased neurofilament density in axons without affecting caliber. *J. Cell Biol.* 111:1543–1557.
Mulligan, L., B.J. Balin, V.M.-Y. Lee, and W.P. Ip. 1991. Antibody labeling of bovine neurofilaments: Implications on the structure of neurofilament sidearms. *J. Struct. Biol.* 106:145–160.
Myers, M.W., R.A. Lazzarini, V.M.-Y. Lee, W.W. Schlaepfer, and D.L. Nelson. 1987. The human mid-size neurofilament subunit: a repeated protein sequence and the relationship of its gene to the intermediate filament gene family. *EMBO (Eur. Mol. Biol. Organ.) J.* 6:1617–1626.
Nagy, A., J. Rossant, R. Nagy, W. Abranow-Newerly, and J.C. Roder. 1993. Derivation of completely cell culture-derived mice from early-passage embryonic stem cells. *Proc. Natl. Acad. Sci. USA*. 90:8424–8428.
Nakagawa, T., J. Chen, Z. Zhang, Y. Kanai, and N. Hirokawa. 1995. The distinct functions of the carboxyl-terminal tail domain of NF-M upon neurofilament assembly: cross-bridge formation and longitudinal elongation of filaments. *J. Cell Biol.* 129:411–429.
Napolitano, E.W., S.S.M. Chin, D.R. Colman, and R.K.H. Liem. 1987. Complete amino acid sequence and in vitro expression of rat NF-M, the middle molecular weight neurofilament protein. *J. Neurosci.* 7:2590–2599.
Nixon, R.A., P.A. Paskevich, R.K. Sihag, and C.Y. Thayer. 1994. Phosphorylation on carboxyl terminus domains of neurofilament proteins in retinal ganglion cell neurons in vivo: influences on regional neurofilament spacing, and axonal caliber. *J. Cell Biol.* 126:1031–1046.
Ohara, O., Y. Gahara, T. Miyake, H. Teraoka, and T. Kitamura. 1993. Neurofilament deficiency in quail caused by nonsense mutation in neurofilament-L gene. *J. Cell Biol.* 121:387–395.
Price, R.L., P. Paggi, R.J. Lasek, and M.J. Katz. 1988. Neurofilaments are spaced randomly in the radial dimension of axons. *J. Neurocytol.* 17:55–62.
Sakaguchi, T., M. Okada, T. Kitarnura, and K. Kawasaki. 1993. Reduced diameter and conduction velocity of myelinated fibers in the sciatic nerve of a neurofilament-deficient mutant quail. *Neurosci. Lett.* 153:65–68.
Schnapp, B.J., and T.S. Reese. 1982. Cytoplasmic structure in rapid-frozen axons. *J. Cell Biol.* 94:667–679.
Shaw, G., and K. Weber. 1982. Differential expression of neurofilament triplet proteins in brain development. *Nature*. 298:277–279.
Shneidman, P.S., M.J. Carden, J.F. Lees, and R.A. Lazzarini. 1988. The structure of the largest murine neurofilament protein (NF-H) as revealed by cDNA and genomic sequences. *Mol. Brain Res.* 4:217–231.
Steinert, P.M., and D.R. Roop. 1986. Molecular and cellular biology of intermediate filaments. *Annu. Rev. Biochem.* 57:593–625.
Tu, P.-H., G. Elder, R.A. Lazzarini, D. Nelson, J.Q. Trojanowski, and V.M.-Y. Lee. 1995. Overexpression of the human NFM subunit in transgenic mice modifies the level of endogenous NFL and the phosphorylation state of NFH subunits. *J. Cell Biol.* 129:1629–1640.
Way, J., M.R. Hellmich, H. Jaffe, B. Szaro, H.C. Pant, H. Gainer, and J. Battey. 1992. A high-molecular-weight squid neurofilament protein contains a lamin-like rod domain and a tail domain with Lys-Ser-Pro repeats. *Proc. Natl. Acad. Sci. USA*. 89:6963–6967.
Willard, M., and C. Simon. 1983. Modulation of neurofilament axonal transport during the development of rabbit retinal ganglion cells. *Cell* 35:551–559.
Wurst, W., and A.L. Joyner. 1993. Production of targeted embryonic stem cell clones. *In* Gene Targeting: A Practical Approach. A.L. Joyner, editor. IRL Press, New York. 33–61.
Xu, Z., D.L.-Y. Dong, and D.W. Cleveland. 1994. Neuronal intermediate filaments: new progress on an old subject. *Curr. Opin. Neurobiol.* 4:655–661.
Xu, Z., J.R. Marszalek, M.K. Lee, P.C. Wong, J. Folmer, T.O. Crawford, S.-T. Hsieh, J.W. Griffin, and D.W. Cleveland. 1996. Subunit composition of neurofilaments specifies axonal diameter. *J. Cell Biol.* 133:1061–1069.
Yamasaki, H., C. Itakura, and M. Mizutani. 1991. Hereditary hypotrophic axonopathy with neurofilament deficiency in a mutant strain of the Japanese quail. *Acta Neuropathol.* 82:427–434.
Yin, X., T.O. Crawford, W. Griffin, P.H. Tu, V.M.-Y. Lee, C. Li, J. Roder, and B.D. Trapp. 1998. Myelin-associated glycoprotein is a myelin signal that modulates the caliber of myelinated axons. *J. Neurosci.* 18:1953–1962.
Zhu, Q., S. Couillard-Depres, and J.-P. Julien. 1997. Delayed maturation of regenerating myelinated axons in mice lacking neurofilaments. *Exp. Neurol.* 148:299–316.
Zopf, D., I. Hermans-Borgmeyer, E.D. Gundelfinger, and H. Betz. 1987. Identification of gene products expressed in the developing chick visual system: characterization of a middle-molecular weight neurofilament cDNA. *Genes Dev.* 1:699–708.